Transient Heat Conduction in On-Chip Interconnects Using Proper Orthogonal Decomposition Method

Banafsheh Barabadi
Department of Mechanical Engineering,
Massachusetts Institute of Technology,
Cambridge, MA 02139

Satish Kumar
G. W. Woodruff School of Mechanical Engineering,
Georgia Institute of Technology,
801 Ferst Drive,
Atlanta, GA 30306

Yogendra K. Joshi
G. W. Woodruff School of Mechanical Engineering,
Georgia Institute of Technology,
801 Ferst Drive,
Atlanta, GA 30306
e-mail: yogendra.joshi@me.gatech.edu

A major challenge in maintaining quality and reliability in today's microelectronics chips comes from the ever increasing levels of integration in the device fabrication, as well as from the high current densities. Transient Joule heating in the on-chip interconnect metal lines with characteristic sizes of tens of nanometer, can lead to thermomechanical fatigue and failure due to the thermal expansion coefficient mismatch between different materials. Full-field simulations of nearly a billion interconnects in a modern microprocessor are infeasible due to the grid size requirements. To prevent premature device failures, a rapid predictive capability for the thermal response of on-chip interconnects is essential. This work develops a two-dimensional (2D) transient heat conduction framework to analyze inhomogeneous domains, using a reduced-order modeling approach based on proper orthogonal decomposition (POD) and Galerkin projection. POD modes are generated by using a representative step function as the heat source. The model rapidly predicted the transient thermal behavior of the system for several cases, without generating any new observations, and using just a few POD modes. [DOI: 10.1115/1.4035889]

Keywords: interconnect, Joule heating, proper orthogonal decomposition, transient thermal analysis

Introduction

Since the 1970s, when the microprocessor became a commercially available and pervasive product, its clock rate has increased by approximately 1×10^6 times. The key to this unprecedented advancement is the scaling of the interconnect wiring and transistor dimensions. With continued scaling, the current density through each wire has increased, while the wire cross section has sharply reduced to the current levels of sub 20 nm. The higher current density has contributed to increased concerns of localized chip heating. The chip and package housing it, experience many thermal cycles for a typical workload environment, causing cyclic stresses that can potentially cause fatigue-related reliability concerns in the interconnects. Experimental and numerical data suggest that the high-operating temperature and high level of thermomechanical stresses are primarily responsible for the morphological changes such as hillocks, whiskers, and voids in the lines that lead to open-circuit and short-circuit failures in interconnects, which limit the quality and reliability of the whole circuit [1,2].

The international technology roadmap for semiconductors (ITRSs) has recognized the importance of transient heat transfer analysis in interconnect reliability. In its 2011 chapter, as well as in 2012 update, it categorizes the challenges in assembly and packaging at feature sizes greater than and below 16 nm. These include integrated analysis tools for transient thermal and thermomechanical analysis.

Joule heating in interconnects has been studied by various methods, both analytically (2D), and numerically using finite difference (FD), and finite element (FE) models [3–6]. The multiscale nature of these configurations results in large computational times with traditional FD and FE methods. This has led to the development of compact thermal models as well as reduced-order techniques that trade resolution and accuracy with shorter computational time, particularly at the interface between the metal and dielectric [7,8]. As addressed previously in the literature [9], the network topography of compact models becomes complex with the increase in model size, potentially also compromising the accuracy of the model. Also, these models have primarily addressed the steady-state Joule heating in interconnects. However, pulsed currents and the resulting transient heat conduction in interconnect arrays remains a key concern in the design for reliability for the next generation high performance chips.

An alternate method for solving the transient heat conduction equation is the transmission line matrix (TLM) approach [10,11]. The TLM formulation is based on a resistance and capacitance network that represents the thermal system. The advantages of this formulation over traditional FE and FD methods are that TLM allows for temperature-dependent and inhomogeneous material parameters, nonuniform meshing, and nonuniform time stepping. Transient Joule heating in copper interconnects embedded in silicon dioxide with constant current density using the TLM and FE methods has been analyzed in Ref. [12]. Also investigated were the effects of the duration and amplitude of rapid square-wave source current pulses [13]. The stability of the results has been shown to be a limitation to this method [12,14]. Furthermore, as the complexity of the structure increases, the simulation times increase, requiring a combination of TLM with multiscale model reduction methods [15].

Model reduction methods have been categorized by Antoulas et al. [16] into two main groups. Methods based on: (1) the singular value decomposition (SVD) and (2) moment matching methods. The most commonly used SVD-based approaches are Hankel-norm approximation [17], singular perturbation [18], and POD [19]. Whereas, Pad′e via Lanczos (PVL) [20], multipoint rational interpolation (a.k.a. rational Krylov algorithm) [21], and implicitly restarted dual Arnoldi [22] are among the popular moment matching methods. Among these techniques, POD is a popular method and can also address highly nonlinear systems

Contributed by the Heat Transfer Division of ASME for publication in the JOURNAL OF HEAT TRANSFER. Manuscript received May 1, 2013; final manuscript received January 25, 2017; published online March 21, 2017. Assoc. Editor: Leslie Phinney.

such as the ones governed by Euler or Navier–Stokes equations without sacrificing the accuracy [23].

In this study, we demonstrate a reduced-order modeling approach based on POD and Galerkin projection technique. The POD is a robust and elegant method of data analysis that enables low-dimensional approximate descriptions of a high-dimensional process. It expands a set of data on empirically determined basis functions for modal decomposition and can be used to numerically predict the temperature distribution more rapidly than full-field simulations. The history of POD goes back over 100 yrs [19], when it was used as a means for processing statistical data. Since that time, it has been applied in many engineering fields, including fluid flow and turbulence [24–26], structural vibrations [27,28], and control theory [29].

More relevant to the theme of this research, POD has been used to analyze micro-electro-mechanical systems (MEMS) and electronic packaging [30,31]. More recently, it has been applied to transient heat conduction problems [32–34]. Bleris and Kothare [35] studied microsystems using empirical eigen-functions obtained from the POD technique to address the problem of thermal transient regulation. A boundary condition (BC) independent POD-Galerkin methodology for 1D heat conduction was studied by Raghupathy et al. [36]. Berkooz et al. [26] provided a thorough summary for applications of POD in various fields. Based on the application, POD can be referred to as principal components analysis (PCA) [37], SVD [38], Karhunen–Lo'eve (KL) decomposition [39], or hotelling transformation [40]. A summary of the equivalence of these three POD methods and the connections among them have been demonstrated by Liang et al. [41].

In this paper, we developed a POD approach implementing the Galerkin projection technique to investigate the transient Joule heating in interconnects in a 2D inhomogeneous system. This study considers the cases with insulated boundary conditions corresponding to the regions embedded in the bulk of a microelectronic device. The effect of different types of current pulses, pulse duration, and pulse amplitude were investigated. The developed POD model can predict the transient temperature distribution, regardless of the temporal dependence of the heat source. This feature of the proposed model provides a predictive capability based on a smaller set of POD modes, which can significantly decrease the computational cost for various transient forcing functions. To validate this unique capability, an analytical proof in 2D was developed (see the Appendix).

Fundamentals of POD Method

POD provides an optimal set of empirical basis functions (also known as POD modes) from an ensemble of observations, obtained either experimentally or numerically. They characterize and capture the overall behavior and complexity of a physical system using a reduced number of degrees-of-freedom (DOF). While the determination of the optimal basis requires some computational effort, the overall cost of the simulations is much lower than full-field simulations. One of the most appealing characteristic of the POD is its *optimality*, i.e., it offers the most efficient method of capturing the dominant components of an infinite-dimensional process with a finite number of modes [42]. This is because, in this technique, data sets are expanded for modal decomposition on empirically determined basis functions, which minimize the least squares error between the true solution and the truncated representation of the POD model [26,43].

The temperature distribution can be determined from the expansion into the POD modes as

$$T(x,y,t) = T_0(x,y) + \sum_{i=1}^{m} b_i(t)\varphi_i(x,y) \tag{1}$$

where T_0 is the time average of temperature (i.e., the mean vector of the observation matrix), $\varphi_i(x, y)$ is the ith POD mode, and $b_i(t)$ is the ith POD coefficient, explained later. The procedure to generate a POD-based reduced-order model is described below.

Generating the Observation Matrix. The initial step in generating the POD observation matrix, T_{Obs}, is to collect a series of observations (also known as snapshots) of temperature distribution at different time instants. The matrix can be formed by collecting the temperature values at n instances of time in the entire domain using either a numerical or experimental approach. Having the ability to utilize experimentally obtained data as the initial observations makes POD a strong candidate to characterize a potentially complex system without generating any numerical model. These initial experimental data can be acquired using thermal sensors within the structure of interest. The spatial accuracy of the POD model will be dependent on the number of sensors placed in the domain. Therefore, based on the desired spatial resolution, proper number of thermal sensors should be utilized. In this study, an FE-based model was used to obtain the initial observation matrix. T_0 in Eq. (1) is the average of all the observed data for any point in the domain. As expected, the accuracy of the POD method depends on the accuracy of the observations. Hence, it is of great importance to perform a grid independence analysis. The other critical factor is to remain above the lowest limit of the number of observations, n, which is problem dependent.

Calculating Basis Functions (POD Modes). Once the observation matrix is produced, the POD modes can be calculated. In Eq. (1), m is the number of POD modes used in the decomposition, which can range from 1 to $n-1$, where n is the number of observations. To determine the POD modes, the method of snapshots is used, where each POD mode is expressed as a linear combination of the linearly independent observations [26]

$$\varphi_i(x,y) = \sum_{k=1}^{n} \beta_{ki}(T_{\text{Obs},k} - T_0) \tag{2}$$

where $T_{\text{Obs},k}$ is the kth column of the observation matrix T_{Obs}, corresponding to the full temperature field at the kth instant of time. As described in Refs. [26] and [44], each eigenvector of the solution of Eq. (3) consists of the weight coefficients β_i

$$\sum \Re\beta = \lambda\beta \tag{3}$$

where λ is the matrix of eigenvalues, and $\Re \in R^{n\times n}$ is the covariance matrix defined as

$$\Re = \frac{1}{n}\left(T^C_{\text{Obs}}\right)^{\text{T}}\left(T^C_{\text{Obs}}\right) \tag{4}$$

where T^C_{Obs} is the *mean-centered observation matrix* obtained by subtracting its mean vector (here T_0), in order to have a zero-mean for the new matrix.

Having calculated the weight coefficients, β, the n POD modes can be determined from Eq. (2). The energy captured by the ith basis function in the problem is relative to its corresponding eigenvalue, λ_i from Eq. (3). Sorting these eigenvalues in a descending order results in an ordering of the corresponding POD modes. Therefore, the first POD mode calculated from Eq. (2) captures the largest portion of energy relative to the other basis functions.

To determine the truncation degree of the POD method, the *cumulative correlation energy*, E_m, captured by the first m POD modes is defined by Bizon et al. [45]

$$E_m = \frac{\sum_{i=1}^{m}\lambda_i}{\sum_{i=1}^{n}\lambda_i} \tag{5}$$

The number of retained POD modes is quite critical in capturing the physics of the problem. It is shown that an insufficient number of the POD modes can cause significant phenomena not to be detected [46]. On the contrary, taking too many POD modes can produce unexpected behavior, or make the model unstable [47]. To be able to generate a reliable POD model, in the present study, the number of POD modes is determined in such a way that the cumulative energy of the modes, calculated from Eq. (5), is larger than 99.99%.

Calculating POD Coefficients, b_i. There are multiple techniques to calculate the POD coefficients b_i for a new test case such as: (1) direct interpolation method [48,49], (2) flux matching process [50,51], (3) radial basis functions (RBFs)-trained POD approach [52,53], and (4) Galerkin projection method [32,54]. The Galerkin projection method is more accurate compared to the other two methods in addressing a time-dependent heat source, since it solves the energy equation for the entire time domain. Therefore, this method is used in this paper.

Galerkin Projection Method. The Galerkin projection method projects the governing equations onto the POD-spanned space. When POD modes are used in a Galerkin projection method, they create a finite-dimensional dynamic system with the smallest possible DOF. In this study, the inhomogeneous transient heat conduction equation is a partial differential equation (PDE). This technique converts this PDE to a set of m-coupled ordinary differential equations (ODEs). The key step in model reduction is to solve a discrete number of coupled ODEs instead of solving a discretized PDE. To further describe the method, we start with the transient heat conduction equation

$$\frac{\partial T}{\partial t} - \frac{1}{\rho c_p} q'''(t) - \alpha \nabla^2 T = 0 \tag{6}$$

where, ρ, c_p, and α are the material density, specific heat capacity, and thermal diffusivity, respectively. $q'''(t)$ is the domain time-dependent volumetric heat generation. Equation (6) is then projected onto the space spanned by POD modes

$$\left\langle \varphi_j, \frac{\partial T}{\partial t} - \frac{1}{\rho c_p} q'''(t) - \alpha \nabla^2 T \right\rangle = 0, j = 1, 2, ..., m \tag{7}$$

where $\langle .,. \rangle$ denoted the inner products, also referred to as the projection of a vector to one another. Using the temperature field from Eq. (1) and integrating Eq. (7) over the entire two-dimensional domain (Ω), we have

$$\int_\Omega \left(\varphi_j, \frac{\partial T}{\partial t} - \frac{1}{\rho c_p} q'''(t) - \alpha \nabla^2 T \right) d\Omega = 0 \tag{8}$$

Discretizing Eq. (8) and using Eq. (1) result in a set of coupled ODEs for the POD coefficients that can be written in a matrix form as

$$A_{ij} \dot{b}_j(t) - B_{ij} b_j(t) - (c + q)_i = 0, i, j = 1, 2, ..., m \tag{9}$$

where $(\dot{})$ denotes the derivative with respect to time. Coefficients A_{ij}, B_{ij}, c_i, and q_i in Eq. (9) are

$$A_{ij} = \int_\Omega \varphi_j \cdot \varphi_i d\Omega \tag{10a}$$

$$B_{ij} = \int_\Omega \alpha \varphi_j \cdot \nabla^2 \varphi_i d\Omega = -\int_\Omega \alpha \left(\frac{\partial \varphi_j}{\partial x} \cdot \frac{\partial \varphi_i}{\partial x} + \frac{\partial \varphi_j}{\partial y} \cdot \frac{\partial \varphi_i}{\partial y} \right) d\Omega + \int_y \left(\alpha \varphi_j \cdot \frac{\partial \varphi_i}{\partial x} \right]_{x=x_{\min}}^{x=x_{\max}} dy + \int_x \left(\alpha \varphi_j \cdot \frac{\partial \varphi_i}{\partial y} \right]_{y=y_{\min}}^{y=y_{\max}} dx \tag{10b}$$

$$c_j = \int_\Omega \alpha \varphi_j \cdot \nabla^2 T_o d\Omega = -\int_\Omega \alpha \left(\frac{\partial \varphi_j}{\partial x} \cdot \frac{\partial T_o}{\partial x} + \frac{\partial \varphi_j}{\partial y} \cdot \frac{\partial T_o}{\partial y} \right) d\Omega + \int_y \left(\alpha \varphi_j \cdot \frac{\partial T_o}{\partial x} \right]_{x=x_{\min}}^{x=x_{\max}} dy + \int_x \left(\alpha \varphi_j \cdot \frac{\partial T_o}{\partial y} \right]_{y=y_{\min}}^{y=y_{\max}} dx \tag{10c}$$

$$q_j = \int_\Omega \frac{1}{\rho c_p} \varphi_j \cdot q'''(t) d\Omega \tag{10d}$$

The last two terms on the right-hand side of Eqs. (10*b*) and (10*c*) are the boundary terms. If the boundary conditions are homogeneous or insulation, these are eliminated, and B_{ij} and c_i are simplified to

$$B_{ij} = -\int_\Omega \alpha \left(\frac{\partial \varphi_j}{\partial x} \cdot \frac{\partial \varphi_i}{\partial x} + \frac{\partial \varphi_j}{\partial y} \cdot \frac{\partial \varphi_i}{\partial y} \right) d\Omega \tag{11a}$$

$$c_j = -\int_\Omega \alpha \left(\frac{\partial \varphi_j}{\partial x} \cdot \frac{\partial T_o}{\partial x} + \frac{\partial \varphi_j}{\partial y} \cdot \frac{\partial T_o}{\partial y} \right) d\Omega \tag{11b}$$

The concept of orthogonality was subsequently applied. Having calculated all the coefficients and substituted those into Eq. (9), these coupled ODEs can be solved using the sixth-order Runge–Kutta method. Notably, the initial conditions for Eq. (9) can be determined by the projection of the POD modes on the initial value for the temperature as

$$b_j^o = b_j(t = 0) = \langle \varphi_j, T(x, y, t = 0) \rangle = 0, \quad j = 1, 2, ..., m \tag{12}$$

Generating the POD Temperature Field. Calculating a sufficient number of POD modes and POD coefficients (b_j and b_j^o) will provide the temperature field from Eq. (1) anywhere in the domain and at any instant of time.

Case Studies

The geometry and topology of on chip interconnects in microelectronic devices can be quite complex. This study focuses on a simplified but realistic 2D model domain. A single interconnect located at the center of a large array of metal lines is considered as shown in Fig. 1. By restricting the problem domain to one corner of this interconnect and the surrounding dielectric material, symmetry arguments can be employed to justify insulated boundary conditions on all sides. This idealized configuration represents the worst thermal scenario, in which the interconnect effectively receives no cooling. This structure approximates long and uniformly spaced interconnects. The interconnect has equal width and height; i.e., the geometrical aspect ratio is 1. The dielectric thickness, H_{de}, is equal to the interconnect height ($H_{de} = H_{int} = 360$ nm). Interconnect pitch P is usually a variable and, in this study, was taken to be $P = 4H_{int} = 1.44$ μm. The initial condition was assumed to be room temperature $T_o = 300$ K. The continuum assumption was verified by calculating the Knudsen number, Kn

$$\text{Kn} = \frac{\Lambda}{L} \tag{13}$$

where Λ is the molecular mean free path, and L is the smallest length scale in the structure [55]. For this structure, the Knudsen number based on the mean free path of electrons in copper at 300 K ($\Lambda = 39$ nm) and the width of interconnects ($H_{int} = 360$ nm) is calculated to be Kn = 0.108. Therefore, the continuum approach is valid. The material properties of the metal and dielectric, representing copper and silicon, were: specific heat capacity $C_p = 380$ and 1000 J/kg K, thermal conductivity $\kappa = 400$ and 0.17 W/m K, and density $\rho = 8933$ and 2200 kg/m^3, respectively.

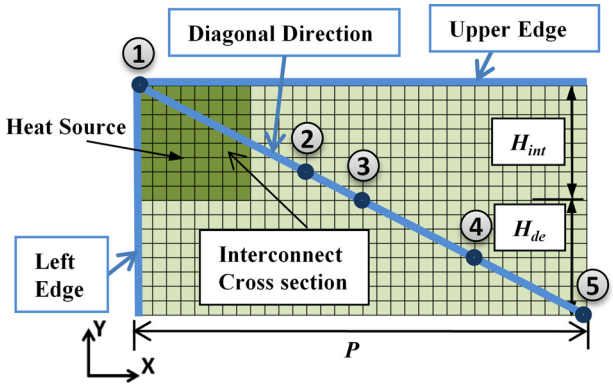

Fig. 1 Schematic of the computational domain with a cross-sectional area of 1.44 μm × 720 nm. It consists of a set of 360 nm × 360 nm interconnects that are evenly spaced and embedded in the dielectric. The mesh used in the POD and FE models is shown. In this study: $H_{int} = H_{de} = 360$ nm and $P = 4H_{int} = 1.44$ μm.

Given that no analytical solution exists for this problem, a detailed FE model was developed in the commercial code LS-DYNA, and the results were used as a basis for the evaluation of the POD modeling approach. The Crank–Nicholson time integration scheme and conjugate gradient iterative solver are chosen for the transient thermal simulations. The results presented here are for $\Delta t = 10.0$ ns. The convergence of the FE model was verified with respect to the solver type, time step, and time integration method. The FE model consists of 561 nodes (17×33) and 512 elements. The grid size was determined based on the mesh independence analysis. For consistency between the FE and the POD models, the same number of nodes at the same position was chosen for the POD model. The top edge, the left edge, and the diagonal of the structure are used in this study for the spatial thermal analysis (Fig. 1); nodes 1–5 on the diagonal are chosen for further temporal thermal analysis of the results. The selection was made based on the directions and positions with the largest value of temperature and temperature gradient.

The effect of current pulse type, pulse duration, and pulse amplitude were investigated in this study. By using a representative step function as the heat source, POD modes are generated. Using just a few POD modes, the model predicted the exact transient thermal behavior of the system for all other cases with different temporal dependence of the heat source and without generating any new observations. Furthermore, the result of the

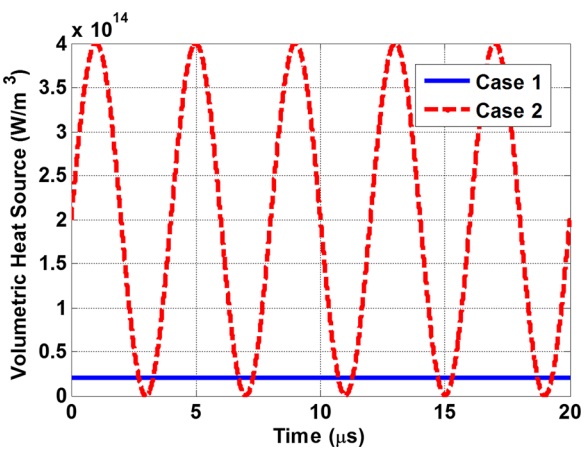

Fig. 2 Different types of heat sources used in this study. Case 1: only step function (solid line) and case 2: sinusoidal and step function (dashed line).

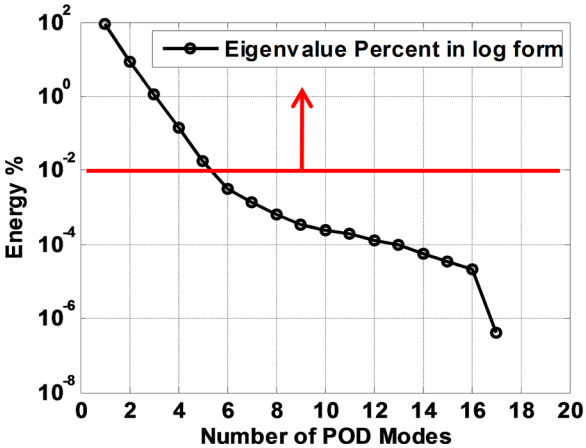

Fig. 3 Eigenvalues or energy percentage in log form versus number of the POD modes. In order to build a reliable reduced order model, the number of basis functions used for the projection was chosen such that the cumulative correlation energy of the modes are greater or equal to 99.99%. The first two modes capture over 98% of the energy.

POD model was compared with a FE model, and a good agreement was found, with a maximum difference of 2%.

To assess the predictive capability of the POD model, two cases corresponding to different thermal scenarios with different time-dependent heat sources were considered. For a better comparison between these cases, a constant value for volumetric heat generation, q'''_0, is calculated based on the current density $J = 10$ MA/cm^2 and the electrical resistivity of $\rho_r = 2.2$ $\mu\Omega$ cm

$$q'''_0 = \rho_r J^2 = 2 \times 10^{13}\ (\mathrm{W/m^3}) \tag{14}$$

Subsequently, the time-dependent heat sources in (W/m^3) for the cases (exhibited in Fig. 2) are

Case 1: $q'''_1 = q'''_0$ (step function with the magnitude of 2×10^{13} W/m^3)

Case 2: $q'''_2 = 10 \times q'''_0 \times [\sin((\pi/2)10^6 t) + 1]$ (combination of a step function with the magnitude of $q'''_2 = 10 \times q'''_0$ and a continuous sinusoidal function, with the period of $\tau_2 = 4$ μs and amplitude of $A_2 = 10 \times q'''_0 = 2 \times 10^{14}$ (W/m^3)

An unwanted surge in the electrical current is represented by case 1, while case 2 represents a condition under which a combination of a sinusoidal noise and a current surge abruptly occur in the interconnect line. The amplitude of the noise in case 2 is ten times higher than, and the frequencies different from, those of case 1. It is of great importance to notice that observations are

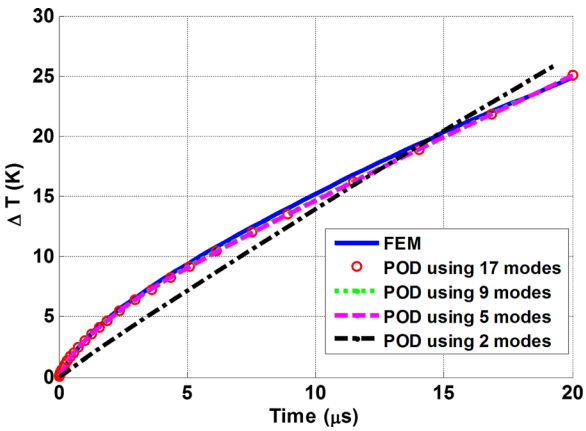

Fig. 4 Comparison of temporal dependence of temperature rise in the left-most node of the top edge (node 1 in the interconnect), $x = 0$ using 17, 9, 5, and 2 observations for case 1

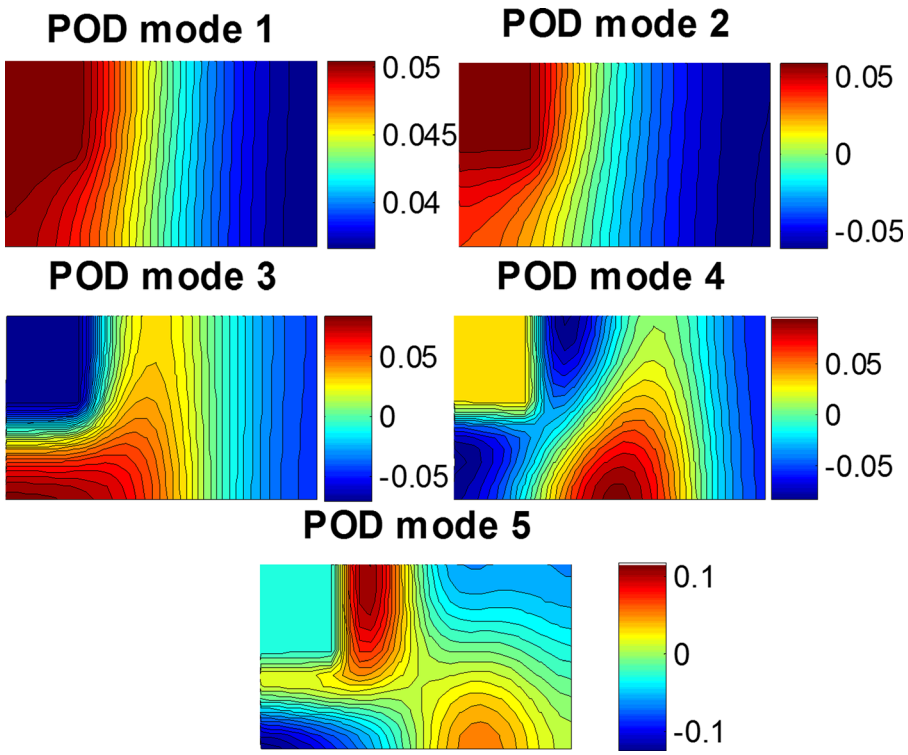

Fig. 5 First five POD modes or basis functions plotted in 2D contours. The POD modes are normalized by the total sum of the modes chosen for each study.

only generated for case 1, and the results of the transient thermal behavior of the second case are determined based on the results obtained from case 1 without generating new observations. This ability of the POD method in predicting thermal behavior of other cases based on a smaller set of modes can significantly decrease the computational cost for the transient analyses. Since the basis functions (∼POD modes) are only dependent on the geometry, the POD modes for any other scenario are the same as for case 1 as long as the governing equations are linear. This distinctive characteristic of POD is proved in the "Appendix" and is numerically confirmed next.

Results and Comparison

Case 1. For $q_1''' = q_0''' = 2 \times 10^{13}$ (W/m^3), 17 observations of the transient temperature using FE simulation were taken in the first 20 μs and were used to calculate the POD modes. The energy percentage for each POD mode is plotted against the mode number in Fig. 3. The magnitude of the eigenvalue and the energy captured by each mode reduces with the index of POD modes. By keeping the first five POD modes, the *cumulative correlation energy*, E_m, was greater than 99.99%. The first two modes, alone, capture over 98% of the energy. For the present study, at least five modes are needed to capture the desired accuracy of 99.99% in the result. If the number of observations, n, were chosen to be less than the minimum required POD modes (here 5), the results will not have the required accuracy. This is demonstrated in Fig. 4 for the temperature rise time history at the top-left-most node (node 1) in case 1 by using 17, 11, 9, 5, and 2 observations. It can be inferred that as long as the number of the observations are more than five, the results are independent of the number of observations, while for the case of 2 observations (dashed–dotted line) the results are not acceptable.

Figure 5 shows the two-dimensional contours of the first five POD modes, normalized based on the total sum of the modes. Using Galerkin projection, described earlier, the POD coefficients were calculated as functions of time. Figure 6 shows the time dependence of the first five b-coefficients. It is apparent that the first coefficients vary in the smoothest way and the coefficients with large indices have large fluctuations during the initial stage. It can also be inferred from Fig. 6 that the value of POD coefficients successively decreases by about an order of magnitude. This shows that only the first few terms in Eq. (1) are dominant and need to be included in the calculations.

Figure 7 shows the contours of the spatial distribution of temperature rise from FE method (top figure) and POD method (bottom picture) after 20 μs for case 1. Over time, heat diffuses from top left, where the source is located, throughout the entire structure. Considering adiabatic boundary condition at all boundaries, the temperature continuously increases in the domain with time, and temperature contours are perpendicular to all the edges. On account of relatively high thermal conductivity and low heat capacity of the copper, temperature gradient within the interconnect cross section is relatively negligible.

To make a more detailed comparison between the POD and FE results, the temperature rise with time at the top-left-most node (node 1), marked in Fig. 1, is considered. Figure 4 demonstrates this comparison for FE (solid line) and POD results using five modes (dashed line) for case 1 in the first 20 μs. As shown in Fig. 4, temperature increases rapidly as the current source is applied. The maximum error between the two models is less than 1%.

As previously mentioned, to show the distinctive capability of the POD model in the prediction of the transient temperature distribution, two cases were considered; case 1 required a new set of observations, while the second case did not need any new observations.

Case 2. In the second case, the capability of the proposed model in predicting the temperature field for a combination of a transient heat pulse and a continuous oscillating source of noise is investigated. The sinusoidal function representing a volumetric heat source, plotted as dashed line in Fig. 2, has a period of $\tau_2 = 4\,\mu$s and amplitude of $A_2 = 10 \times q_o''' = 2 \times 10^{14}$ (W/m^3). There are no new generated observations for this case. Figure 8

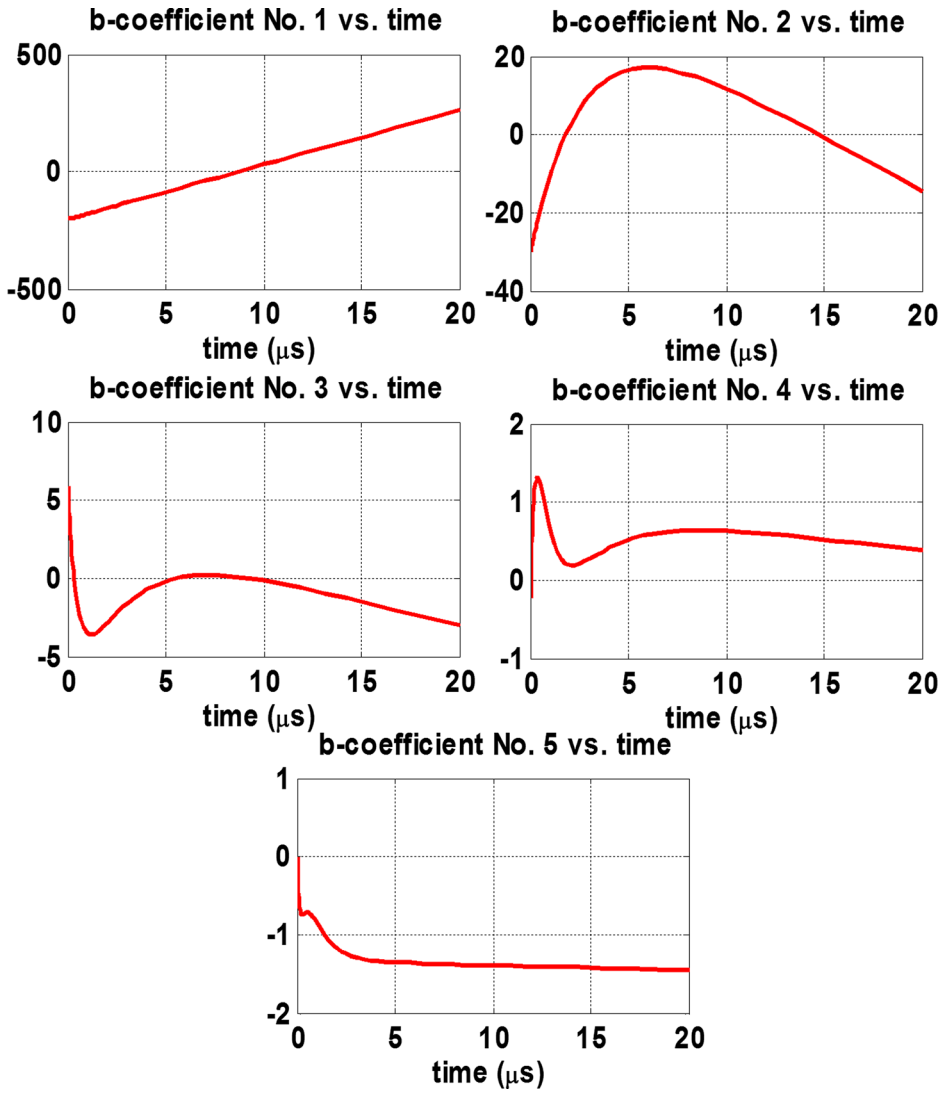

Fig. 6 First five *b*-coefficients versus time using the Galerkin projection technique for case 1

shows the temperature rise at several locations for case 2. FE results and POD results using five basis functions are shown at two different times. Figures 8(*a*), 8(*c*), and 8(*e*) for time = 18 μs corresponds to a time slightly before the first crest in the fifth cycle of the heat source, while Figs. 8(*b*), 8(*d*), and 8(*f*), at 19.2 μs, simulates a time slightly after the bottom of the sinusoidal curve in the fifth cycle. Figures 8(*a*)–8(*f*), also, demonstrate that the difference between the two models decreases in both x and y directions, as distance from the heat source increases (for lower values of x and for higher values of y). The regions on the graphs with negligible temperature gradient correspond to the location of the interconnect. A maximum truncation error of less than 1.5% exists between the two models. The computation time required for the POD simulation is up to two orders of magnitude smaller than that of the full field FE simulation. Since majority of the run-time is spent on the generation of the POD modes, once the first POD simulation is performed, any additional simulations to study different power sources take even shorter time. This is because, for any additional run, only the POD coefficients need to be determined. The computations were performed on a workstation using an Intel(R) Core (TM) i7 at 2.20 GHz with 8 GB RAM. Therefore, once the effort has been expended in building a POD model, it can then be used to carry out computationally low cost parametric studies in optimization of a design.

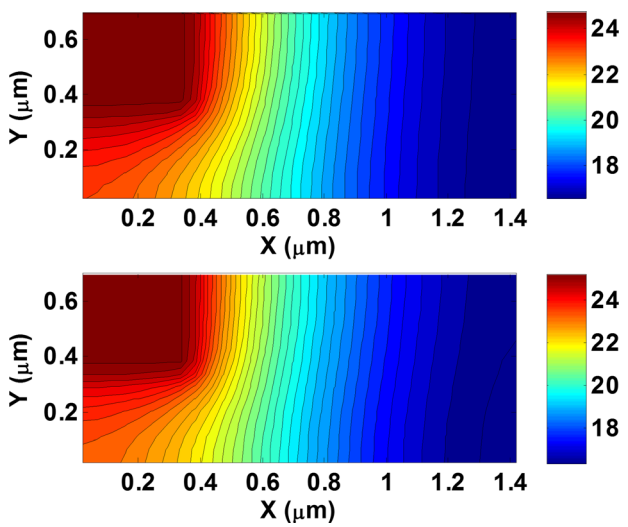

Fig. 7 Spatial variation of temperature rise after 20 μs for FE (top) and POD (bottom) models using five basis functions for case 1

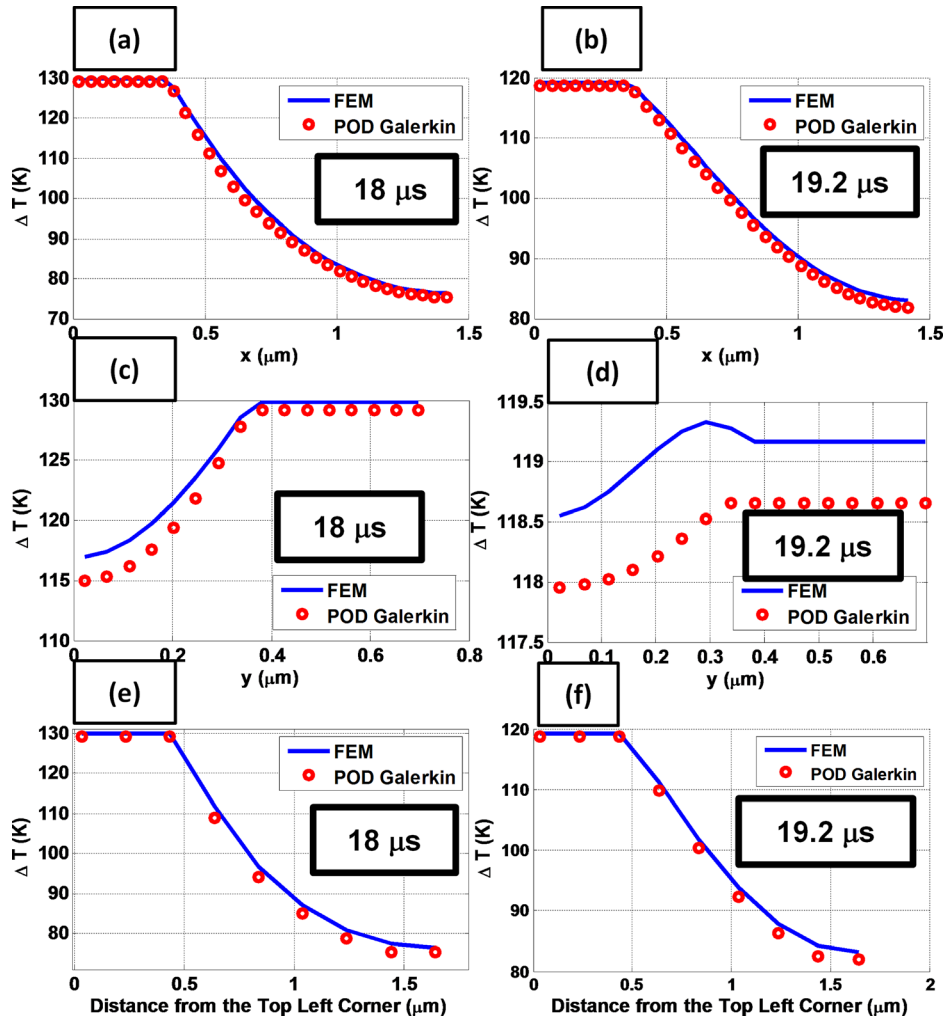

Fig. 8 Spatial variation of temperature rise after 18 μs in *x* direction for the upper edge of the structure (*a*), *y* direction for the left edge of the structure (*c*), and along the diagonal (*e*). Spatial variation of temperature after 19.2 μs in *x* direction for the upper edge of the structure (*b*), *y* direction for the left edge of the structure (*d*), and along the diagonal (*f*). The FE results are plotted in solid lines, and the POD results using five basis functions are plotted in circular markers. The results are for case 2.

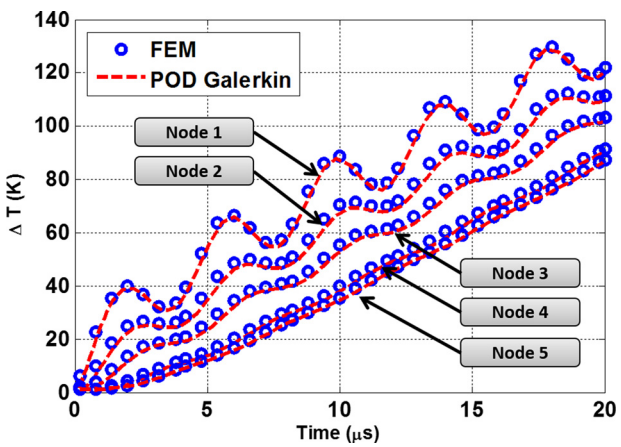

Fig. 9 Comparison of temporal dependence of temperature rise at nodes 1–5 along the diagonal for case 2. The FE results are plotted in circular markers, and the POD results are shown by dashed lines.

A comparison of temperature rise between FE (circular markers) and POD (solid lines) models of nodes 1–5 along the diagonal (noted in Fig. 1) is provided for case 2 in Fig. 9. Based on the results presented for case 2, it can be interpreted that our POD model using Galerkin projection technique can predict the transient thermal behavior for a single sinusoidal heat wave. These results further confirm the ability of the POD with Galerkin projection technique to predict the transient thermal behavior of this structure for any temporal dependent heat source, based on a single available observation matrix. Other types of heat sources such as step functions and sinusoidal functions with different frequencies and amplitude were also investigated and verified [56]. This capability of POD is further confirmed through an analytical proof of a 2D transient problem provided in the Appendix.

Conclusion and Discussion

In this study, the POD method and Galerkin projection technique were implemented to address the transient Joule heating in a two-dimensional inhomogeneous arrangement of interconnects embedded in a dielectric material. Insulated boundary conditions were considered, representing the worst thermal scenario in regions of microelectronic devices where the interconnects in fact receive no cooling. The developed POD model works best for

scenarios with either adiabatic or periodic boundary conditions. The model, however, can be further improved by including more complicated boundary conditions.

A sufficient number of POD modes can be easily estimated which will contain the most energy. The POD modes are obtained at the system level using the observations from FE model. The number of POD modes kept in the analysis is determined in such a way that the cumulative energy of the modes was larger than 99.99% of the total energy. The POD coefficients were subsequently calculated using the method of Galerkin projection.

To assess the POD predictions, two time-dependent heat source conditions were considered. In both cases, the POD model predictions were in good agreement with the corresponding FE models. The computational time of POD model is up to two orders of magnitude smaller than that of a tradition FE analysis. The truncation errors calculated based on the difference of the POD and FE model were found to be less than 2%. The results show that the truncation error does not increase as the amplitude of the heat source increases. Moreover, the POD modes are not sensitive to the temporal dependence of the heat source. It was also demonstrated that the POD model accurately predicted the transient thermal behavior of the system for not only the time domain considered for the initial observations but also for time outside the specified initial domain. These important features can drastically decrease computational cost, making POD a robust method in modeling transient heat conduction in microelectronic devices which can then be used to carry out computationally low cost parametric studies in optimization of a design.

Nomenclature

A = heat wave amplitude (W/m^3)
A_{ij} = coefficient in Eq. (9)
b = POD coefficient (K)
B_{ij} = coefficient in Eq. (9)
c_i = coefficient in Eq. (9)
c_p = specific heat (J/kg K)
E_m = cumulative correlation energy
f = constant spatial function
H = height (m)
J = current density (MA/cm^2)
Kn = Knudsen number
L = smallest length scale in the structure (m)
m = number of POD modes used
n = number of observations
q_i = coefficient in Eq. (9)
$q'''(t)$ = volumetric heat generation (W/m^3)
T = temperature (K)
X = arbitrary function of x
Y = arbitrary function of y
∇^2 = Laplace operator
$\langle .,. \rangle$ = inner product of two functions
$()''$ = second spatial derivative
$(\dot{})$ = time derivative

Greek Symbols

α = thermal diffusivity (m^2/s)
β = weight coefficients
γ = arbitrary constant
Γ = time dependent coefficients
δ = arbitrary constant
Θ = the basis functions
κ = thermal conductivity (W/m K)
λ = eigenvalue
Λ = molecular mean free path (nm)
μ = arbitrary constant
Π = time dependent coefficients, Eq. (A6)
ρ = density (kg/m^3)
ρ_r = electrical resistivity ($\mu\Omega$ cm)
τ = heat wave period (μs)
φ = POD mode
Ω = two-dimensional domain
$\Re$ = covariance matrix

Subscripts

de = dielectric
int = interconnect
obs = observation

Superscripts

C = mean centered
o = initial value

Appendix: Analytical Proof

Here, we show that the POD modes for the same geometry will not change by changing the temporal dependence of the heat source. The transient heat equation is considered (Eq. (A1))

$$\frac{\partial T(x,y,t)}{\partial t} - \frac{1}{\rho c_p} q'''(x,y,t) - \alpha \nabla^2 T(x,y,t) = 0 \tag{A1}$$

with homogeneous boundary conditions (BCs)

$$\left.\frac{\partial T(x,y,t)}{\partial x}\right|_{y=0} = 0 \tag{A2a}$$

$$\left.\frac{\partial T(x,y,t)}{\partial y}\right|_{x=0} \mathrm{s} = 0 \tag{A2b}$$

and initial condition

$$T(x,y,t=0) = f(x,y) = \text{const} \tag{A2c}$$

First, the case where $q'''(x,y,t) = 0$ is considered. For this case, Eq. (A1) is simplified to

$$\frac{\partial T(x,y,t)}{\partial t} = \alpha \nabla^2 T(x,y,t) \tag{A3}$$

Since Eq. (A3) is a homogeneous PDE with homogeneous BCs, the method of eigenfunction expansion can be applied to solve for $T(x, y, t)$ as

$$T(x,y,t) = \sum_r \sum_s \Gamma_{rs}(t) \Theta_{rs}(x,y) \tag{A4}$$

where $\Theta_{rs}(x,y)$ are the basis functions. $\Gamma_{rs}(t)$ are the time-dependent coefficients that can be found by projecting $T(x,y,t)$ onto the basis vectors $\Theta_{rs}(x,y)$. Ultimately, using the method of separation of variables, the temperature field can be written as

$$T(x,y,t) = \sum_r \sum_s \Gamma_{rs}(t) X_r(x) Y_s(y) \tag{A5}$$

Once the basis functions for the homogeneous equation (Eq. (A3)) are determined, we look at the original nonhomogeneous equation (Eq. (A1)) which includes the source term $q'''(x,y,t)$. The basis functions are assumed to be the same for both homogeneous and nonhomogeneous PDEs. In other words, the source term $q'''(x,y,t)$ can also be expanded into the same basis functions for temperature; i.e., $X(x)$ and $Y(y)$, because $q'''(x,y,t)$ stays in the same Hilbert space as $T(x,y,t)$. Hence, the source term can be written as

$$q'''(x,y,t) = \sum_r \sum_s \Pi_{rs}(t) X_r(x) Y_s(y) \tag{A6}$$

Now that the basis functions are the same for both of Eqs. (A1) and (A3), the time-dependent coefficients $\Pi_{rs}(t)$ in Eq. (A6) can be found by projecting $q'''(x,y,t)$ onto the basis vectors $\Theta_{rs}(x,y)$ as

$$\Pi(t) = \langle X(x)Y(y), q'''(x,y,t) \rangle \tag{A7}$$

The derivatives of temperature, $\partial^2 T(x,y,t)/\partial x^2$, $\partial^2 T(x,y,t)/\partial y^2$, and $\partial T(x,y,t)/\partial t$, are calculated from Eq. (A5) and substituted into Eq. (A1) which yields to

$$\begin{aligned} &\sum_r \sum_s \frac{\partial \Gamma_{rs}(t)}{\partial t} X_r(x) Y_s(y) \\ &+ \alpha \left(\sum_r \sum_s \mu_r^2 \Gamma_{rs}(t) X_r(x) Y_s(y) + \sum_r \sum_s \gamma_r^2 \Gamma_{rs}(t) X_r(x) Y_s(y) \right) \\ &- \frac{1}{\rho C_P} \sum_r \sum_s \Pi_{rs}(t) X_r(x) Y_s(y) = 0 \end{aligned} \tag{A8}$$

Simplifying this equation provides

$$\sum_r \sum_s \left[\frac{\partial \Gamma_{rs}(t)}{\partial t} + \alpha \Gamma_{rs}(t) \left(\mu_r^2 + \gamma_s^2 \right) - \frac{1}{\rho C_P} \Pi_{rs}(t) \right] \times X_r(x) Y_s(y) = 0 \tag{A9}$$

Applying the orthogonality condition to the basis functions $X(x)$ and $Y(y)$ results in

$$\frac{\partial \Gamma_{rs}(t)}{\partial t} + \alpha \Gamma_{rs}(t) \left(\mu_r^2 + \gamma_s^2 \right) - \frac{1}{\rho C_P} \Pi_{rs}(t) = 0 \tag{A10}$$

To find Γ_{rs}^0, the initial condition for Γ_{rs}, we apply Eq. (A5) into the initial condition for the temperature, (Eq. (A2*c*)) as

$$\begin{aligned} f(x,y) = T(x,y,t=0) &= \sum_r \sum_s \Gamma_{rs}(t=0) X_r(x) Y_s(y) \\ &= \sum_r \sum_s \Gamma^0{}_{rs} X_r(x) Y_s(y) \end{aligned} \tag{A11}$$

where Γ_{rs}^0 can be determined by projecting $f(x,y)$ onto the basis functions $X(x)$ and $Y(y)$ as

$$\Gamma_{rs}^0(t) = \langle X_r(x) Y_s(y), f(x,y) \rangle \tag{A12}$$

Once $\Gamma^0{}_{rs}$ is determined, Eq. (A10) can be solved for Γ_{rs} in the entire domain. The discussed arguments demonstrate the reasoning behind the fact that once the POD modes are determined for the homogeneous problem, the source term (nonhomogeneity) can be written in the form of a summation of the POD modes obtained originally. Hence, by varying the time dependency of the heat source in our problem there would be no need for any further observation generation.

References

[1] Lloyd, J. R., and Thompson, C. V., 1993, "Materials Reliability in Microelectronics," MRS Bull., **18**(12), pp. 16–18.

[2] Phan, T., Dilhaire, S., Quintard, V., Lewis, D., and Claeys, W., 1997, "Thermomechanical Study of AlCu Based Interconnect Under Pulsed Thermoelectric Excitation," J. Appl. Phys., **81**(3), p. 1157.

[3] Bilotti, A. A., 1974, "Static Temperature Distribution in IC Chips With Isothermal Heat Sources," IEEE Trans. Electron Devices, **21**(3), pp. 217–226.

[4] Shen, Y. L., 1999, "Analysis of Joule Heating in Multilevel Interconnects," J. Vac. Sci. Technol., B: Microelectron. Nanometer Struct., **17**(5), pp. 2115–2121.

[5] Teng, C. C., Cheng, Y. K., Rosenbaum, E., and Kang, S. M., 2002, "Item: A Temperature-Dependent Electromigration Reliability Diagnosis Tool," IEEE Trans. Comput.-Aided Des. Integr. Circuits Syst., **16**(8), pp. 882–893.

[6] Chen, D., Li, E., Rosenbaum, E., and Kang, S. M., 2002, "Interconnect Thermal Modeling for Accurate Simulation of Circuit Timing and Reliability," IEEE Trans. Comput.-Aided Des. Integr. Circuits Syst., **19**(2), pp. 197–205.

[7] Stan, M. R., Skadron, K., Barcella, M., Wei, H., Sankaranarayanan, K., and Velusamy, S., 2003, "Hotspot: A Dynamic Compact Thermal Model at the Processor-Architecture Level," Microelectron. J., **34**(12), pp. 1153–1165.

[8] Gurrum, S. P., Joshi, Y. K., King, W. P., Ramakrishna, K., and Gall, M., 2008, "A Compact Approach to On-Chip Interconnect Heat Conduction Modeling Using the Finite Element Method," ASME J. Electron. Packag., **130**(3), p. 031001.

[9] Celo, D., Ming, G. X., Gunupudi, P. K., Khazaka, R., Walkey, D. J., Smy, T., and Nakhla, M. S., 2005, "Hierarchical Thermal Analysis of Large IC Modules," IEEE Trans. Compon. Packag. Technol., **28**(2), pp. 207–217.

[10] Christopoulos, C., 2002, "The Transmission-Line Modeling Method: TLM," IEEE Antennas Propag. Mag., **39**(1), p. 90.

[11] De Cogan, D., O'connor, W. J., and Pulko, S., 2005, *Transmission Line Matrix (TLM) in Computational Mechanics*, CRC Press, Boca Raton, FL.

[12] Barabadi, B., Joshi, Y. K., Kumar, S., and Refai-Ahmed, G., 2010, "Thermal Characterization of Planar Interconnect Architectures Under Transient Currents," ASME Paper No. IMECE2009-11996.

[13] Barabadi, B., Joshi, Y. K., Kumar, S., and Refai-Ahmed, G., 2010, "Thermal Characterization of Planar Interconnect Architectures Under Different Rapid Transient Currents Using the Transmission Line Matrix and Finite Element Methods," 12th IEEE Intersociety Conference on Thermal and Thermomechanical Phenomena in Electronic Systems (ITherm), Las Vegas, NV, June 2–5, pp. 1–8.

[14] Ait-Sadi, R., and Naylor, P., 1993, "An Investigation of the Different TLM Configurations Used in the Modelling of Diffusion Problems," Int. J. Numer. Modell.: Electron. Networks, Devices Fields, **6**(4), pp. 253–268.

[15] Smy, T., Walkey, D., and Dew, S., 2001, "Transient 3d Heat Flow Analysis for Integrated Circuit Devices Using the Transmission Line Matrix Method on a Quad Tree Mesh," Solid-State Electron., **45**(7), pp. 1137–1148.

[16] Antoulas, A., Sorensen, D., and Gugercin, S., 2001, "A Survey of Model Reduction Methods for Large-Scale Systems," Contemp. Math., **280**(2001), pp. 193–220.

[17] Glover, K., 1984, "All Optimal Hankel-Norm Approximations of Linear Multivariable Systems and Their L,∞-Error Bounds†," Int. J. Control, **39**(6), pp. 1115–1193.

[18] Kokotovic, P. V., 1976, "Singular Perturbations and Order Reduction in Control Theory—An Overview," Automatica, **12**(2), pp. 123–132.

[19] Pearson, K., 1901, "LIII on Lines and Planes of Closest Fit to Systems of Points in Space," London, Edinburgh, Dublin Philos. Mag. J. Sci., **2**(11), pp. 559–572.

[20] Feldmann, P., and Freund, R. W., 1995, "Efficient Linear Circuit Analysis by Padé Approximation Via the Lanczos Process," IEEE Trans. Comput.-Aided Des. Integr. Circuits Syst., **14**(5), pp. 639–649.

[21] Grimme, E. J., 1997, "Krylov Projection Methods for Model Reduction," Ph.D. thesis, University of Illinois at Urbana-Champaign, Champaign, IL.

[22] Jaimoukha, I. M., and Kasenally, E. M., 1997, "Implicitly Restarted Krylov Subspace Methods for Stable Partial Realizations," SIAM J. Matrix Anal. Appl., **18**(3), pp. 633–652.

[23] Tan, B. T., 2003, "Proper Orthogonal Decomposition Extensions and Their Applications in Steady Aerodynamics," Ph.D. thesis, Ho Chi Minh City University of Technology, Ho Chi Minh, Vietnam.

[24] Ahlman, D., Jackson, J., Kurdila, A., and Shyy, W., 2002, "Proper Orthogonal Decomposition for Time-Dependent Lid-Driven Cavity Flows," Numer. Heat Transfer, Part B, **42**(4), pp. 285–306.

[25] Berkooz, G., Holmes, P., and Lumley, J. L., 1993, "The Proper Orthogonal Decomposition in the Analysis of Turbulent Flows," Annu. Rev. Fluid Mech., **25**(1), pp. 539–575.

[26] Berkooz, G., Holmes, P., and Lumley, J., 1996, "Turbulence, Coherent Structures, Dynamical Systems and Symmetry," *Cambridge Monographs on Mechanics*, Cambridge University Press, New York, pp. 1200–1208.

[27] Cusumano, J. P., Sharkady, M. T., and Kimble, B. W., 1994, "Experimental Measurements of Dimensionality and Spatial Coherence in the Dynamics of a Flexible-Beam Impact Oscillator," Philos. Trans. R. Soc., A, **347**(1683), pp. 421–438.

[28] Feeny, B. F., and Kappagantu, R., 1998, "On the Physical Interpretation of Proper Orthogonal Modes in Vibrations," J. Sound Vib., **211**(4), pp. 607–616.

[29] Atwell, J. A., and King, B. B., 2001, "Proper Orthogonal Decomposition for Reduced Basis Feedback Controllers for Parabolic Equations," Math. Comput. Modell., **33**(1–3), pp. 1–19.

[30] Liang, Y., Lin, W., Lee, H., Lim, S., Lee, K., and Sun, H., 2002, "Proper Orthogonal Decomposition and Its Applications—Part II: Model Reduction for MEMS Dynamical Analysis," J. Sound Vib., **256**(3), pp. 515–532.

[31] Codecasa, L., D'amore, D., and Maffezzoni, P., 2003, "An Arnoldi Based Thermal Network Reduction Method for Electro-Thermal Analysis," IEEE Trans. Compon. Packag. Technol., **26**(1), pp. 186–192.

[32] Bialecki, R., Kassab, A., and Fic, A., 2005, "Proper Orthogonal Decomposition and Modal Analysis for Acceleration of Transient FEM Thermal Analysis," Int. J. Numer. Methods Eng., **62**(6), pp. 774–797.

[33] Bialecki, R., Kassab, A., and Fic, A., 2003, "Reduction of the Dimensionality of Transient FEM Solutions Using Proper Orthogonal Decomposition," AIAA Paper No. 2003-4207.

[34] Fic, A., Bialecki, R. A., and Kassab, A. J., 2005, "Solving Transient Non-Linear Heat Conduction Problems by Proper Orthogonal Decomposition and FEM," Numer. Heat Transfer, Part B, **48**(2), pp. 103–124.

[35] Bleris, L. G., and Kothare, M. V., 2005, "Reduced Order Distributed Boundary Control of Thermal Transients in Microsystems," IEEE Trans. Control Syst. Technol., **13**(6), pp. 853–867.
[36] Raghupathy, A. P., Ghia, U., Ghia, K., and Maltz, W., 2010, "Boundary-Condition-Independent Reduced-Order Modeling of Heat Transfer in Complex Objects by POD-Galerkin Methodology: 1d Case Study," ASME J. Heat Transfer, **132**(6), p. 064502.
[37] Jolliffe, I. T., and Myilibrary, 2005, *Principal Component Analysis*, Springer, New York.
[38] Grossman, R. L., and Kamath, C., 2001, *Data Mining for Scientific and Engineering Applications*, Kluwer Academic Publishers, Norwell, MA.
[39] Kirby, M., and Sirovich, L., 2002, "Application of the Karhunen-Loeve Procedure for the Characterization of Human Faces," IEEE Trans. Pattern Anal. Mach. Intell., **12**(1), pp. 103–108.
[40] Eriksson, P., Jiménez, C., Bühler, S., and Murtagh, D., 2002, "A Hotelling Transformation Approach for Rapid Inversion of Atmospheric Spectra," J. Quant. Spectrosc. Radiat. Transfer, **73**(6), pp. 529–543.
[41] Liang, Y., Lee, H., Lim, S., Lin, W., Lee, K., and Wu, C., 2002, "Proper Orthogonal Decomposition and Its Applications—Part I: Theory," J. Sound Vib., **252**(3), pp. 527–544.
[42] Holmes, P., Lumley, J. L., and Berkooz, G., 1998, *Turbulence, Coherent Structures, Dynamical Systems and Symmetry*, Cambridge University Press, New York.
[43] Chatterjee, A., 2000, "An Introduction to the Proper Orthogonal Decomposition," Curr. Sci., **78**(7), pp. 808–817.
[44] Rolander, N. W., 2005, "An Approach for the Robust Design of Data Center Server Cabinets," Ph.D. thesis, Georgia Institute of Technology, Atlanta, GA.
[45] Bizon, K., Continillo, G., Russo, L., and Smula, J., 2008, "On POD Reduced Models of Tubular Reactor With Periodic Regimes," Comput. Chem. Eng., **32**(6), pp. 1305–1315.
[46] Graham, M. D., and Kevrekidis, I. G., 1996, "Alternative Approaches to the Karhunen-Loeve Decomposition for Model Reduction and Data Analysis," Comput. Chem. Eng., **20**(5), pp. 495–506.
[47] Rowley, C. W., Colonius, T., and Murray, R. M., 2001, "Dynamical Models for Control of Cavity Oscillations," AIAA Paper No. 2001-2126.
[48] Ding, P., Wu, X. H., He, Y. L., and Tao, W. Q., 2008, "A Fast and Efficient Method for Predicting Fluid Flow and Heat Transfer Problems," ASME J. Heat Transfer, **130**(3), p. 032502.
[49] Ly, H. V., and Tran, H. T., 2001, "Modeling and Control of Physical Processes Using Proper Orthogonal Decomposition," Math. Comput. Modell., **33**(1), pp. 223–236.
[50] Rambo, J., and Joshi, Y., 2007, "Reduced-Order Modeling of Turbulent Forced Convection With Parametric Conditions," Int. J. Heat Mass Transfer, **50**(3–4), pp. 539–551.
[51] Rambo, J. D., 2006, "Reduced-Order Modeling of Multiscale Turbulent Convection: Application to Data Center Thermal Management," Ph.D. thesis, Geogia Institute of Technology, Atlanta, GA.
[52] Ostrowski, Z., Białecki, R., and Kassab, A., 2008, "Solving Inverse Heat Conduction Problems Using Trained POD-RBF Network Inverse Method," Inverse Probl. Sci. Eng., **16**(1), pp. 39–54.
[53] Ostrowski, Z., Białecki, R. A., and Kassab, A. J., 2005, "Estimation of Constant Thermal Conductivity by Use of Proper Orthogonal Decomposition," Comput. Mech., **37**(1), pp. 52–59.
[54] Temam, R., 1997, *Infinite Dimensional Dynamical Systems in Mechanics and Physics*, Springer, New York.
[55] Zhang, Z. M., 2007, *Nano/Microscale Heat Transfer*, McGraw-Hill Professional, New York.
[56] Barabadi, B., Joshi, Y., and Kumar, S., 2011, "Prediction of Transient Thermal Behavior of Planar Interconnect Architecture Using Proper Orthogonal Decomposition Method," ASME Paper No. IPACK2011-52133.